2.2 Vacuum Vessel

2.2.1 Function and Main Components

The primary functions of the vacuum vessel (VV) are to provide a high quality vacuum for the plasma, as well as the first confinement barrier of radioactive materials and a second barrier (after the cryostat) for the separation of air from potential sources of in-vessel hydrogen generation. The decay heat of all the in-vessel components can be removed by the water in the VV primary heat transfer system (PHTS) system, even in conditions when the other PHTSs are not functioning. The vessel supports in-vessel components and their loads during normal and off-normal operation. In addition, a tight fitting configuration of the VV to the plasma aids the plasma vertical stability, and the ferromagnetic material in the VV reduces the toroidal field ripple. Along with other in-vessel components, the VV provides adequate radiation shielding, in particular for the magnets and to allow access to the cryostat and port connections two weeks after shutdown.

The main components that make up the VV are the main vessel and the port structures.

The VV is a permanent machine component (RH class 3) and is safety classified (SIC).

2.2.2 Vacuum Vessel Design

2.2.2.1 Overall Arrangement

The VV is a torus-shaped, double wall structure with shielding and cooling water between the shells. The VV is located inside the cryostat and supported by the vessel gravity supports from the toroidal field (TF) coil case (see Figure 2.2-1); these are provided as part of the magnet system.

The blanket and divertor are mounted on the vessel interior and all loads are transferred to the vessel. The blanket modules are supported directly by the VV and the blanket cooling channels are routed over its plasma-side surface (see 2.3). The basic configuration and poloidal cross-section of the VV are shown in Figures 2.2-2 and -3, respectively. Detailed parameters are summarized in Table 2.2-1.

The VV has upper, equatorial, and lower port structures used for equipment installation, utility feedthroughs, cryo-vacuum pumping, and access inside the vessel for maintenance. Most of the port components are also of double wall construction with stiffening ribs between the walls.

The VV components need to be designed and manufactured consistent with an accepted code or standard. In addition, the design, materials and manufacturing of the VV components need to be consistent with providing a high quality vacuum.

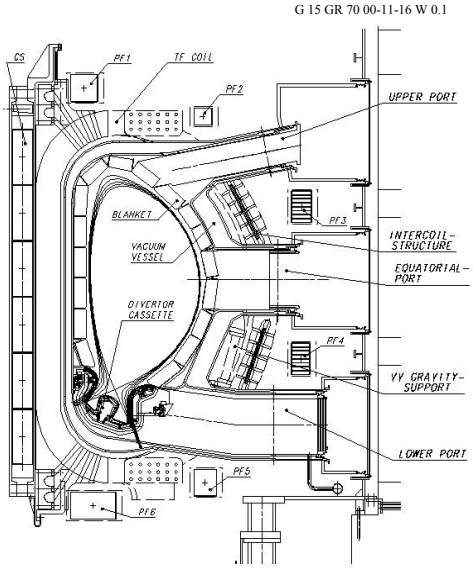

Figure 2.2-1
Tokamak Poloidal Cross-Section

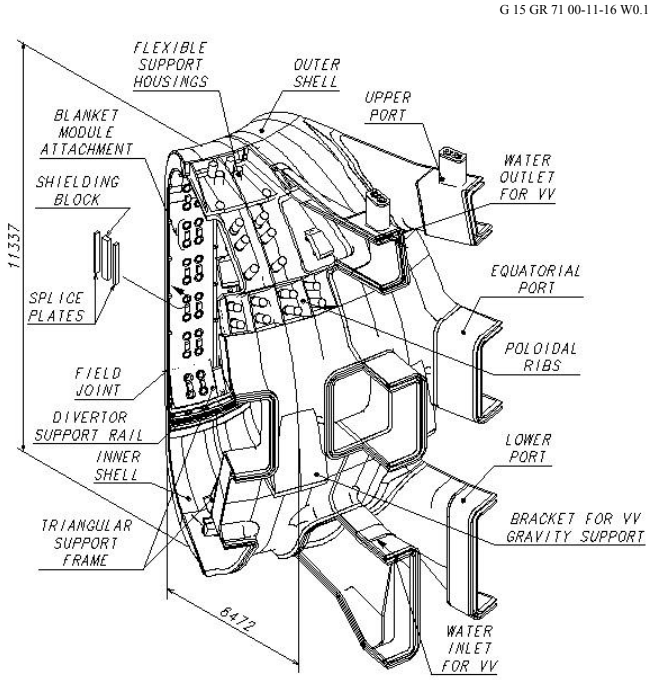

Figure 2.2-2
Vacuum Vessel Overall Arrangement

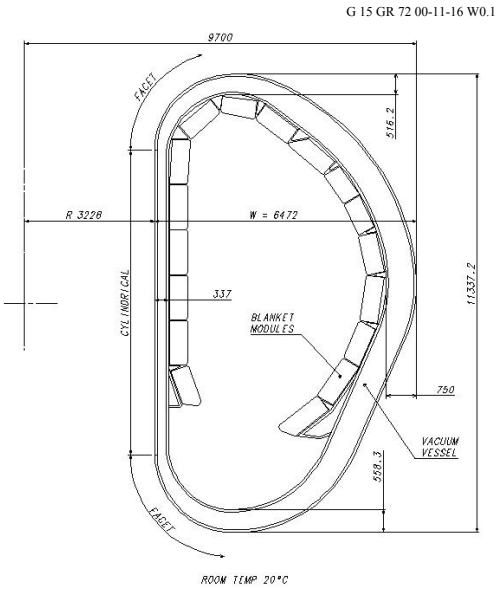

Figure 2.2-3
Vacuum Vessel Cross-Section

Table 2.2-1 Main VV Parameters

Size	
- Toroidal Extent of Sector	40°
- Shell Thickness	60 mm
- Rib Thickness	40 mm
Structure	
- Inboard Straight Region	Cylindrical
- Inboard Top/Bottom	Faceted
- Outboard Region	Faceted
Resistance	
- Toroidal	7.9 μΩ
- Poloidal	4.1 μΩ
Required Leak Rate	1×10^{-8} Pam^{-3}/s
Surface Area / Volume	
- Interior Surface Area	939 m^2
- Interior Volume	1,598 m^3
- Structural Volume (cooling channel)	639 m^3
Materials	
- Main Vessel and Port Structures	SS 316L(N)-IG
- Primary Shielding	SS 30467
- Ferromagnetic Insert Shielding	SS 430
- Connecting Ducts	SS 304
Mass (without water)	
- Main Vessel (without shielding)	2,542 t
- Shielding	2,889 t
- Port Structures	1,967 t
- Connecting Ducts	1,050 t
- Total	8,448 t

2.2.2.2 Materials

The choice of the materials used for the VV has a significant influence on costs, performance, maintainability, licensing, detailed design parameters, and waste disposal. The primary reason for the choice of materials shown in Table 2.2-1 is their high mechanical strength at operating temperatures, water chemistry properties, excellent fabrication characteristics, and low cost relative to other candidates.

The space between the double wall will be filled with shield structures mainly made of an austenitic stainless steel containing 2 weight % boron. The addition of boron to SS 304 was adopted to improve neutron shielding efficiency. A ferritic stainless steel is used as the shielding material under the TF coils in the outboard area to reduce toroidal field ripple. This steel has a high saturated magnetization at ~ 1.7 T. Both the materials have high corrosion resistance in water and excellent fabrication characteristics.

2.2.3 Vacuum Vessel Component Description

2.2.3.1 Main Vessel

The main vessel consists of inner and outer shells, ribs, shield structures, splice plates, shielding structures for field joints, and mechanical structures on the inner and outer shells to support in-vessel components and to support the vessel weight (see Figure 2.2-2).

The double wall structure has stiffening ribs between the shells to give the required mechanical strength and separate the shells. The number of ribs is minimized to simplify the vessel design and to reduce the cost. The basic vessel design is an all-welded structure. The inner and outer shells and stiffening ribs are joined by welding. The inner and outer shells are both 60 mm plates and the stiffening ribs mainly 40 mm plate. The shells and ribs form the flow passages for the vessel cooling water (see 2.2.4). The space between the shells will be filled with shielding.

The heavy steel structure of the VV provides a reliable first confinement barrier. Although the VV is a double wall structure, the inner shell serves as the first confinement barrier.

The VV is divided toroidally into 9 sectors joined by field welding using splice plates at the central vertical plane of alternate ports. The structure of the sector field joint will allow two sector replacement cycles and accommodate a mismatch between adjacent vessel sectors. Each sector includes a full set of port stubs and stub extensions at the toroidal centre of the sector and a set of half port stubs (split on the port centre) on each side. The straight sections of the inboard form a cylinder, and transitions are made to a four-facet per sector design at the top and bottom of this cylindrical section.

The VV is supported by VV gravity supports which minimize the tangential toroidal displacement of VV ports during each pulse (see 2.1).

A "tight fitting" configuration of the VV to the plasma has been employed to position the plasma-facing surface of the blanket modules in the correct position. The tight fitting vessel, together with the toroidally continuous triangular support frames for the lower blanket modules, also aids plasma vertical stability (Figure 2.2-2). The triangular support frames are needed also to provide the structural integrity of the VV.

Each blanket module is attached directly to the VV (or the triangular support frame) by a set of four flexible supports located symmetrically with respect to the module centre (see 2.3). The flexible supports are mounted in housings that are recessed into the VV (Figure 2.2-4). Where flexible support housings occur in the VV double wall structure, stiffening ribs between the shells are partially replaced by housings, which are connected between the inner and outer shells. The double wall structure continues around the housing to maintain the inner shell as the first confinement barrier (Figure 2.2-4). In addition, the module support structures include centring-keys and shear-keys for the inboard, and stub-keys for the outboard modules (see 2.3). The direct attachment of the modules to the VV produces local stresses due to poloidal/radial forces and moments, mainly generated in the modules by plasma disruptions and vertical displacement events (VDEs). To withstand these forces and moments, the vessel shells need to be locally reinforced by toroidal and poloidal ribs in the inboard region where the forces and moments are largest. Poloidal reinforcement ribs are locally connected between the support housings and to the inner shell, while toroidal reinforcement ribs are also used between the housings but they are not connected to the shells so as not to disturb the water flow. The poloidal reinforcement ribs strengthen the inner shell also against the forces from the shear-keys.

The blanket cooling manifolds (see 2.3) are supported on the VV by brackets that are welded to the vessel inner shell by a set of supports which distribute the reaction force from the manifolds to a wide surface, minimizing the local shear stress in the vessel shell.

G 15 GR 74 00-11-16 W0.1

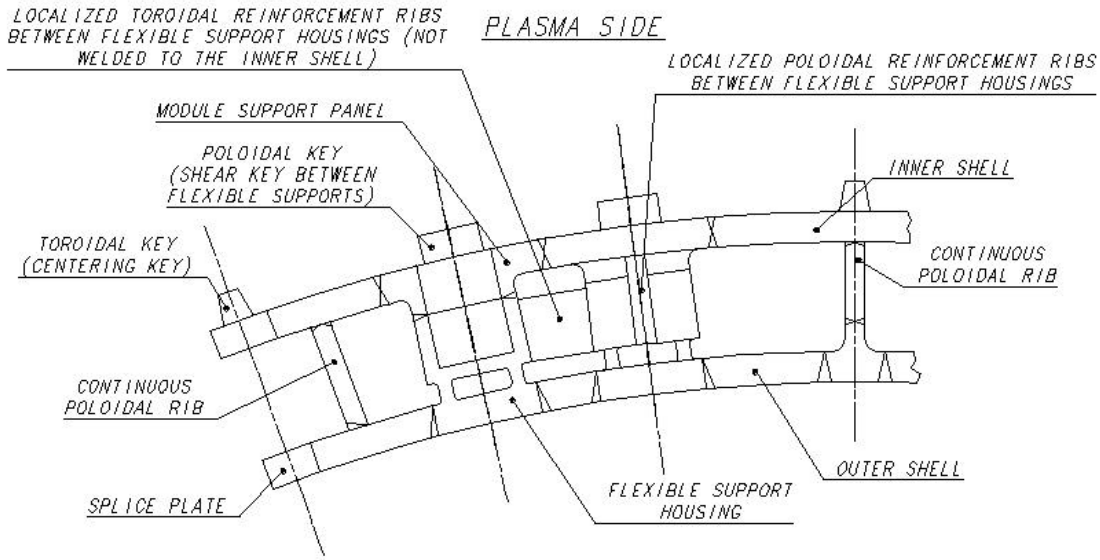

Figure 2.2-4 Typical Toroidal Cross-Section at Inboard Region

In addition to the blanket modules, divertor cassettes are supported by the VV (Figures 2.2-1 and 2) on toroidal rails at the inboard and outboard regions and by radial rails for the three divertor remote handling ports during remote maintenance (see 2.4 and 2.9). Because of the required precise alignment of the cassettes, these rails are installed after the VV is completed in the pit.

To provide adequate neutron shielding, the space between the vessel shells is filled, up to 60%, with steel plates (Figures 2.2-5 to 7). Where ferromagnetic steel is used as the shielding material under the TF coil in the outboard area (12 o'clock to 5 o'clock except the equatorial port region), these plates fill up to 80% of the volume between the shells to reduce toroidal field ripple by about a factor of 2. 40 mm thick plates will be used. Individual shielding plates are bolted together to form shields (Figure 2.2-7). The shields are fixed by bolts and pins to the ribs or module support housings to withstand the mechanical forces. The gaps between the shields and between the shields and the ribs are minimized to avoid excess neutron streaming. The shields for the field joints must be assembled on site and removed if replacement of the TF coil and vessel sector is required. The structure is a three-part shield that can be totally disassembled and removed from the field joint area, maximizing space available for welding, cutting, and inspection equipment.

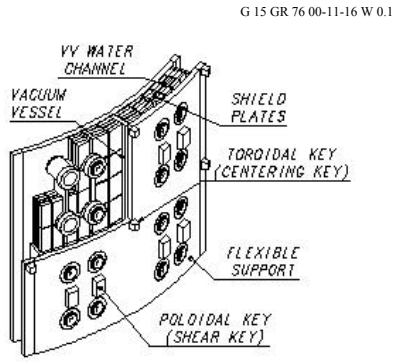

Figure 2.2-5
Arrangement of Shields

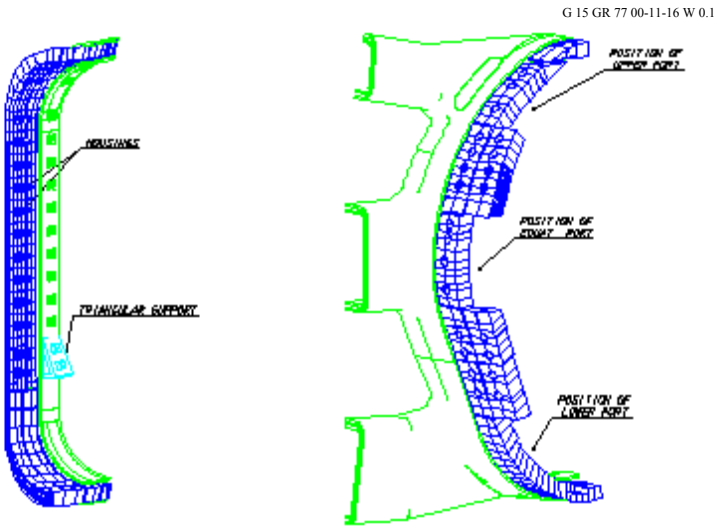

Inboard Region Outboard Region

Figure 2.2-6 Layout of Shields

The vessel is a passive component. There will however be instrumentation to monitor vessel and cooling water temperature, water pressure, local vessel stress/strain, and dynamic movement using thermocouples, pressure gauges, strain gauges and acceleration sensors (see 2.2.6).

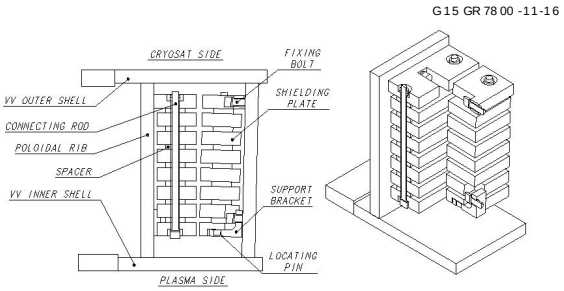

Figure 2.2-7 Structure of Shields

2.2.3.2 Port Structures

The vacuum vessel has upper, equatorial, and lower port structures that will be used for equipment installation, utility feedthroughs, cryo-vacuum pumping, and access inside the vessel for maintenance. A typical port structure includes a port stub and a port extension. The port extensions are normally equipped with the closure plates (on the extension end), which provide the primary vacuum boundary. The port stub is welded to the main vessel at the machine assembly station and the port extension is welded to the port stub in the pit. The port extensions are connected to the cryostat by connecting ducts that are a part of the secondary vacuum boundary. The basic port arrangement is shown in Figure 2.2-8. A summary of the port usage and inside dimensions is given in Table 2.2-2.

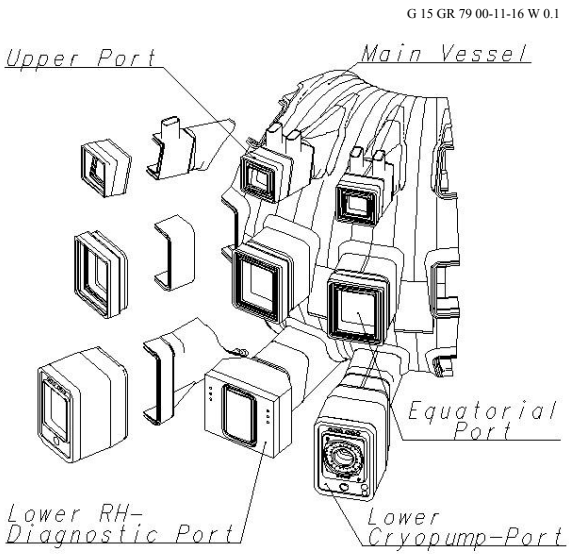

Figure 2.2-8 Port Arrangement

Table 2.2-2 Summary of Port Arrangement

Port Type	Number of Ports	Inside Dimensions (m)
Upper		
- Diagnostics, EC Systems, VV/Blanket Water Piping	18	0.835 to 1.154 (width) x 1.16 (height)
Equatorial		
- Regular (RH/Port Limiter, RF Heating Systems, Diagnostics, Test Blanket Modules)	14*	1.748 (width) x 2.2 (height)
- Heating Neutral Beam	2	0.582 (width) x 1.256 (min. height)
- Heating/Diagnostic Neutral Beam	1	0.582 (width) x 1.256 (min. height) 0.404 (width) x 0.438 (min. height)
Lower		
- RH/Diagnostics, VV/Divertor Piping	5	0.728 to 1.39 (width) x 2.175 (height)
- Cryopumps, IVV Systems, VV/Divertor Piping	13	0.728 to 1.39 (width) x 2.175 (height)

* There is no standard equatorial port next to the first NB port due to limited access for the RH equipment in this area.

The upper ports are inclined upwards and have a trapezoidal cross-section in the area between the TF coils, that is transformed to a rectangular cross-section beyond the coils. The pipes for the VV water outlet are welded to the port outer surface. The blanket pipes run along the port inner surface and exit the port through chimneys located at the port top before the closure plate. Feedthroughs for the helium purge pipes for the breeding blanket also follow this routing.

For the upper ports, the in-port components and the closure plate are integrated into one subassembly. The in-port component, which occupies the space delimited by the blanket pipes, is supported as a cantilever from the end portion of the port extension through the VV closure flange. There are tangential keys to withstand torque moments and the bolted flange joint to withstand all other loads (Figure 2.2-9). The tangential keys are located at the corners of the flange (4-8 keys in total). The keys are adjustable to compensate fabrication/assembly tolerances. The vacuum/pressure seal is made with a lip-welded joint which is incorporated into the bolted flange. The lip seal structure allows repeated cutting/rewelding for the in-port component replacement.

The equatorial ports include regular ports and neutral beam (NB) ports. The regular ports are radial and have a rectangular cross-section. As in the upper port, the in-port components and the port closure plate are integrated. The NB ports provide an angled access for the neutral beams for plasma heating and current drive. The NB ports are situated in three adjacent sectors of the machine and comprise 2 heating ports and a combined heating/diagnostic beam port. The port structure extends to the interface points with the cryostat and the NB system. The NB port has inner liners located along it, cooled by the blanket cooling water, to cope with the nuclear heating and the radiation of the plasma and the beam. A massive shield is integrated with the port or main vessel walls to enhance local shielding. Additional but similar structures are required for the plasma diagnostic neutral beam.

The lower ports are inclined downwards and have a trapezoidal cross-section in the area between the TF coils, which transforms to a rectangular cross-section beyond the coils. Each of the 3 RH/diagnostic ports is equipped with a removable closure plate and has a rectangular-box structure at the end to accommodate diagnostic waveguides. The closure plate of these ports is bolted to the port extension with a lip seal joint as in the upper port.

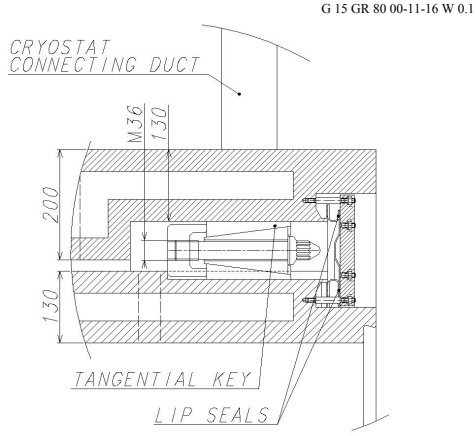

Figure 2.2-9
Support Structure of Port Flange

For the cryopump port, the cryopump and the closure plate are integrated into one subassembly. The port end plate has a large opening for the cryopump closure plate and a small opening at the bottom for the in-vessel viewing access. The cryopump closure plate is either bolted to the port end plate with a lip seal joint or welded to the end plate with a thick weld.

All lower ports are equipped with pipe stubs for the VV cooling water inlet connections and draining pipes. In addition, the divertor coolant pipe feedthroughs penetrate the port end plate.

The port stubs, extensions, and liners are of double wall structure with stiffening ribs between the walls. The connecting ducts have a single-wall construction. The double wall port components are cooled or baked by the VV water flowing between the shells. The total thickness of the port stubs and extensions is normally 200 mm (130 mm as the minimum) and the shell thickness is 60 mm or 40 mm. The NB port components generally require a thicker wall to enhance the port shielding properties. Steel plates may be incorporated between the walls of some ports to enhance local shielding.

2.2.4 Cooling and Baking

Performance differences between the VV and blanket require the use of separate cooling water circuits. Heat deposited in the vacuum vessel during normal and off-normal operations will be removed by cooling water that is supplied by the VV primary heat transfer system (see 3.3). Two independent water loops with the same cooling capability are used in each of the 9 sectors, feeding all sectors in parallel. Table 2.2-3 summarizes the VV cooling and baking conditions.

During normal operation, the design value of the total heat deposition in the VV is mainly due to nuclear heating. The heat is non-uniformly deposited in the VV. In addition, high heat deposition is also expected in the neutron-streaming regions, such as between blanket modules. The non-uniformly distributed heat in the VV is to be removed without any local overheating of the VV. During an off-normal event, e.g., a multiple cooling pump trip in the

blanket cooling system, the main heat load to be considered is thermal radiation from the blanket/divertor.

The water flow velocity and mass flow rate for normal operation need to cope with the nuclear heating rate in the VV in such a way that will keep thermal stresses in the VV structure at acceptable levels. The required water flow condition for normal and baking operation is forced turbulent flow. In order to maintain stresses at acceptable levels for the blanket manifold, the VV cooling water inlet temperature difference with respect to the blanket cooling water inlet temperature has to remain limited (~50˚) for normal and baking operations. During off-normal operation, the decay heat of both the VV and blanket would be removed by the water that is circulated by thermo-gravitational convection due to the heat flux from the vessel wall to the water (i.e., natural convection).

Table 2.2-3 Cooling and Baking Conditions of the Vacuum Vessel

Parameters	Value
Maximum Heating Power	
- Normal Operation (MW)	10
- Off-normal Operation (Decay Heat) (MW)	0.83
Number of Loops of VV PHTS	2
Normal Operation	
- Cooling Mode	Forced Convection (mainly)
- Water Mass Flow Rate for Two Loops (kg/s)	950
- Water Inlet Temperature (°C)	100
- Temperature Rise (°C)	2.5
- Water Inlet Pressure (MPa)	1.1
Off-normal Operation*	
- Cooling Mode	Natural Convection
- Water Mass Flow Rate for Two Loops (kg/s)	40
- Temperature Rise (°C)	5
Baking Operation	
- Water Inlet Temperature (°C)	200
- Water Inlet Pressure (MPa)	2.4

*: Assuming two loops are in operation to remove the decay heat of 0.83 MW.

The basic flow arrangement for the vessel is shown in Figure 2.2-10. The cooling water is supplied and flows through the lower ports and is routed to an internal supply manifold structure at the bottom of each sector. This manifold distributes the water to channels on both the inboard and outboard sides of the vessel to provide a uniform flow rate in the channels. The water flows up and is collected in an internal manifold at the top of the vessel and is routed through a channel in the upper port wall to an exit point. This configuration was selected to provide a system with maximum natural convection cooling to remove decay heat during off-normal operation. Water is also supplied from the main vessel to the triangular support structure.

Figure 2.2-11 shows water flow passages for the inboard region. Since about 70 % of the heat is deposited in the inner shell and the first shield plate during normal operation, the flow route is designed to allow the water to flow mainly through the gap between them. The heat deposited in this region is removed by forced convection of the water which provides sufficient heat removal capability (more than 500 $W/m^2/K$ of heat transfer coefficient). However, the heat deposited in the triangular support structures will be removed mainly by natural convection.

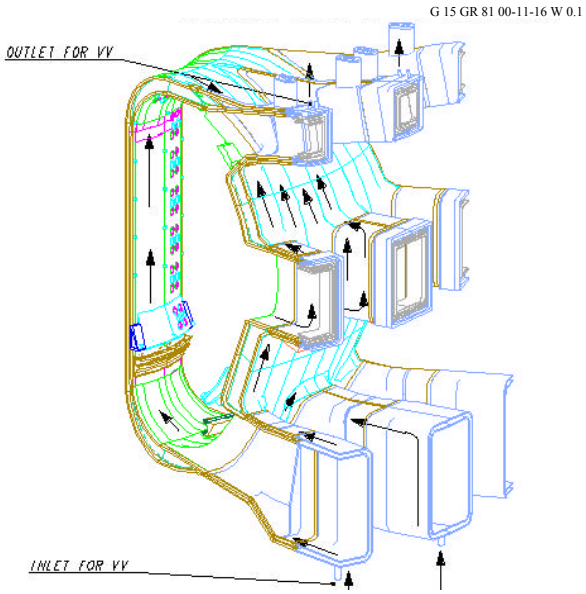

Figure 2.2-10
VV Water Routing

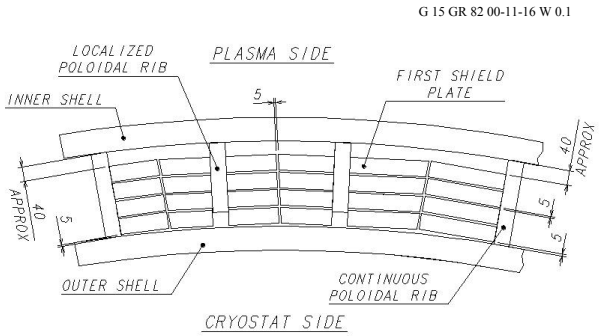

Figure 2.2-11
Water Flow Passage for
Inboard Region (Toroidal section)

2.2.5 Fabrication

To minimize the final assembly time on site, and to deliver a vessel structure with a high quality, the VV is to be fabricated in the factory as 9 sectors each spanning 40°. The practicality of transporting such a large sector from the factory to the site is an important factor in the manufacture of the vessel and must be assessed after the site is selected. The port stubs on the lateral sides of the sector are not installed in the factory. This allows the TF coils to be installed in the assembly area (discussed in 2.2.6).

The shields are installed at the factory before shipment to the site for all circuits except in the area of the field joints. In addition, most of the instrumentation and devices for coolant distribution for blanket modules are installed and experimentally examined at the factory.

Two concepts have mainly been considered for the sector fabrication scheme (Figure 2.2-12). One is to complete the inner shell first because it forms the first confinement boundary. Butt weld joints can be fully applied to the inner shell and inspection can be easily performed. Next, all ribs and support housings would be welded to the inner shell. After shields have been installed, parts of the outer shell would be welded (access is from the rib side and through the open space). The remaining parts of the outer shell would be welded (with a one-sided weld). Another concept is to utilize poloidal segments of a double wall structure, which are fabricated first then welded together to form a sector. This scheme was employed for the full-scale vessel sector fabrication in the L-3 R&D project[1]. In addition to the two schemes, an alternative scheme based on the mixture of the two schemes can be considered. Poloidal segments of a vessel without the outer shells are to be completed first. After the segments are welded together to form a poloidally closed shape, the outer shells will be welded.

[1] K. Koizumi, et al., "Design and Development of the ITER Vacuum Vessel, Fusion Engineering and Design," 41 (1998) 299-304, and K. Koizumi, et al., "Development of double-walled vacuum vessel for ITER," Proc. 16th IAEA Fusion Energy Conference, Montreal, Canada, October 1996, Vol.3, pp.845-852.

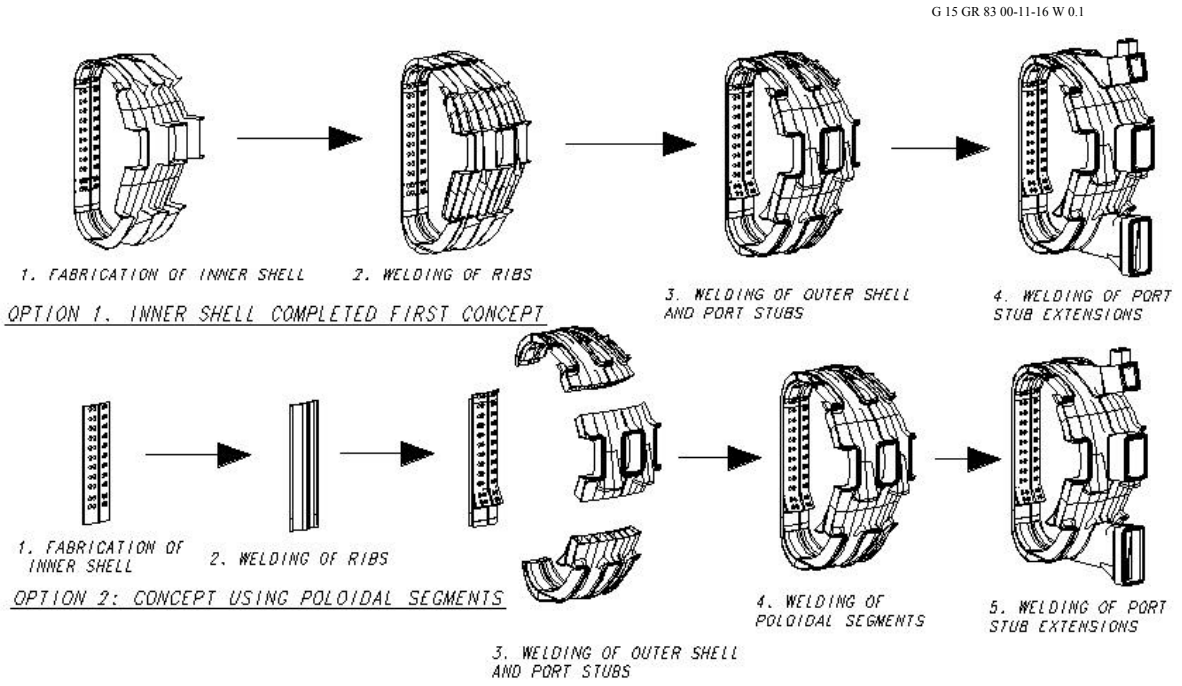

Figure 2.2-12 Options for Fabrication of a VV Sector

Figures 2.2-4 and 13 shows an example of the inboard region including the weld joint configurations and the inboard assembly procedure. Most weld joints have conventional configurations and can be radiographically inspected to assure 100% weld efficiency. It is considered that they could be easily code/standard qualified. However, the one-sided weld joints between the outer shell and the ribs and the field joints will be inspected mainly by UT (ultrasonic testing).

Some fabrication and inspection aspects of the vessel are not consistent with the rules of the applied code, and exceptions (called code cases) must be developed and approved. The currently considered code cases for the VV are: (1) the one-sided weld joint design of the outer shell to the stiffening ribs, (2) the one-sided field weld joint design of the vessel sector to the splice plates, (3) the special stainless steel 316L(N)-IG to be used as the fabrication material, and (4) the wish not to use dye penetrant at cut edges, welds, and peripheral base metal surfaces on the vacuum side. Qualification of the VV fabrication/inspection and the code cases depends on the ITER host country and the applied codes/standards.

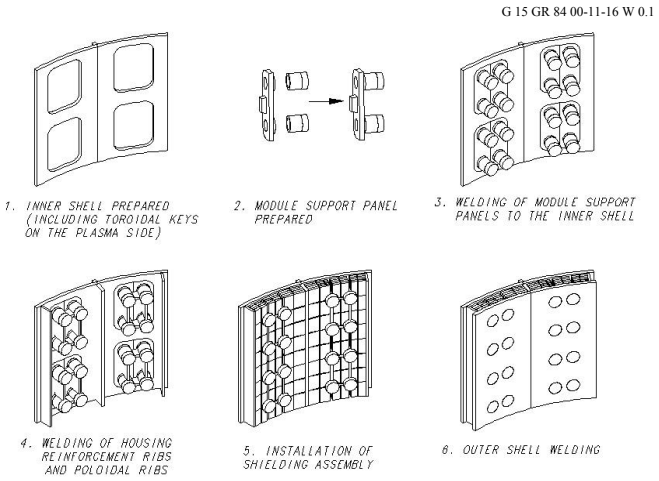

Figure 2.2-13
Fabrication Procedure of VV Inboard Region

To reduce the VV fabrication cost, a forged and/or cast structure has been investigated. For example, the region of the VV gravity support is a highly-stressed region, requiring numerous

reinforcements. Instead of an all-welded shell structure, a forged structure would reduce the fabrication cost and improve the fabrication tolerances. Currently, a thick outer shell made by forging is considered in the region between the equatorial ports where the VV gravity support is mounted. In addition, the large number of housings in the VV for the blanket module support that have a relatively small and simple structure can be manufactured by precision casting for cost saving. Powder HIPing is also being considered for further cost reduction.

The most important VV R&D performed during the EDA was associated with the fabrication of a sector and demonstration of remote welding, cutting and NDT systems. The full scale sector model, fabricated and tested as a part of the L-3 project, provided critical information related to fabrication technology required to produce a high quality sector, and the magnitude of welding distortions and achievable tolerances. Since the basic design of the ITER VV is the same as the fabricated sector model (i.e., the material, the basic torus shape, and the double wall structure with shielding and cooling water between the shells), this R&D also validated the fundamental feasibility of the ITER double wall design. Additional R&D, such as the fabrication of a partial VV sector model, may be required to confirm the improved fabrication technology and associated tolerances, as a first step to be done by the industrial firm chosen for manufacturing the vacuum vessel.

2.2.6 Initial Assembly, Commissioning, and Maintenance

At the ITER site, each sector is mated to two TF coils (and thermal shield) and assembled. Sector/coil mating involves moving a TF coil over each end of the sector. The lateral port stub halves are then welded in place. After the sector/coils are lowered into and positioned in the pit, 9 field joints (located on the centre of the lateral ports) are TIG-welded using splice plates to compensate for the size differences of the sectors. The final machine assembly sequence involves a sequential attachment of adjacent sectors until the resulting 160° and 200° segments are finally joined (see 2.10). Before VV commissioning is complete, the pressure boundary must be pressure tested as required by the code.

The advantages of the proposed VV sector geometry, versus one relying on one shop-manufactured sector per TF coil, result from the reduction in operations and associated requirements. The three most important benefits of assembling this larger sector are (1) the reduction of assembly cost by reducing the number of field joints, (2) improved dimensional stability due to the reduction in field joint welding, and (3) the capability to install in shop all additional piping, etc. inside the VV. In addition, the proposed VV sector geometry provides simple water routings for the VV and blanket modules in the VV structure, and full port structures at the toroidal centre of the sector.

An in-service inspection (ISI) program is not required by design codes, which signify only code-compliant construction. In particular, monitoring the vacuum pressure and mass spectrum in the VV and in the cryostat is expected to satisfy the objective of ISI. Very small leaks through the VV structure, which do not affect the VV structural integrity, can be detected and may also degrade plasma performance. In addition, there will be instrumentation to monitor the VV system status, particularly the vessel and cooling water temperature, water pressure, local vessel stresses/strains, and dynamic movement. As a further measure of investment protection, temperature, pressure stresses/strains or accelerations deviating from set point values will terminate plasma operation.

2.2.7 Design Criteria, Loads and Analyses

2.2.7.1 Design Criteria for the VV

The VV loading events and combinations have been classified into categories (see 2.12). These events are further classified into different service levels A, B, C or D which relate to the damage limits (A: negligible damage, functional; B: negligible damage, maintenance may be needed; C: local distortion possible, repair or replacement may be needed; D large non-local distortion possible, but minimum safety function maintained, and replacement may be needed; these are usually abbreviated to normal, upset, emergency, and faulted, respectively). The VV has been designed in accordance with ASME VIII div.2 for the normal operational design loads (category I and II events). For the events of category III and IV, not covered by ASME VIII, rules and safety factors as specified in ASME III have been used. Table 2.2-4 summarizes the service levels and the stress intensity "k" factors which are used to define the allowable stress.

Table 2.2-4 Design Criteria for Vacuum Vessel

Loading Event Category	Service Level	Damage Limit	Stress Intensity "k" Factor
I Operational	A	Normal	1.0
II Likely	A	Normal	1.0
III Unlikely	C	Emergency	1.2
IV Extremely unlikely	D	Faulted	2.0 (1)

Note:
1. As given in Table ASME III Subsection NC-3217-1 Note 4 the stress limit of Appendix F (fault conditions) may be applied, allowing a "k" value of 2.4.

The allowable stresses for the various types of stress (primary, membrane, bending, etc.) as defined by ASME VIII div.2 appendix 4 are computed as follows:

General Primary Membrane	$< 1.0\ k\ S_m$
Local Primary Membrane	$< 1.5\ k\ S_m$
Primary Membrane + Bending	$< 1.5\ k\ S_m$
Primary + Secondary	$< 3.0\ k\ S_m$ (only for Category I and II)

2.2.7.2 Load Description and Values

The VV must withstand many individual and combined loading conditions during both normal and off-normal operation.

Table 2.2-5 reports the list of the operating states to be considered for the design of the VV. Table 2.2-6 reports the list of the load case combination and the category and the Service Limit Levels. The ICEs have to be combined with disruptions and VDEs, but the time scale evolution of the over-pressure and over-temperature caused by the ingress of water is much longer than the time scale evolution of the EM loads and does not occur at the same time.

Different types of VDEs are considered based on the speed of the plasma current quench (slow=S and fast=F) and on the direction of the plasma movement (downward=D or upward=U). These VDEs are named VDE/S-D, VDE/S-U, VDE/F-D, and VDE/F-U.

Table 2.2-5 VV Design Load Events and Categories

Operating State	ITER Load Category	Service Limit Level (per ASME Code)
1) Construction	I	A
2) Testing		
2a) Pressure test 1 (Coolant Pressure)	Test	Test
2b) Pressure test 1 (VV Internal Pressure)	Test	Test
2c) Pressure test 1 (VV External Pressure)	Test	Test
3) Off State	I	A
4) Baking State	I	A
5) Normal Plasma Operating State		
5a) Centre Disruption (CD) I (54 ms)	I	A
5b) Centre Disruption (CD) II (27 ms)	II	A
5c) Vertical Displacement Event (VDE) I	I	A
5d) Vertical Displacement Event (VDE) II	II	A
6) Ingress of Coolant Event (ICE) II	II	A
7) Toroidal Field Coil Fats Discharge (TFCFD)	I	A
8) Maintenance State	I	A
9) Seismic SL-1	II	A
10) Vertical Displacement Event (VDE) III	III	C
11)Overpressure States		
11a) ICE III (Pressure Pulse in-vessel breach < 0.1 m^2)	III	C
11b) ICE IV (Pressure Pulse in-vessel breach < 0.6 m^2)	IV	C
11c) Cryostat Air Ingress	III	C
11d) Cryostat Water Ingress	IV	C
12) Over-temperature states		
12a) VV loss of (forced) flow (one loop) + VV ex-vessel coolant leak (one loop)	IV	D
13) Seismic SL-2	IV	D
14) Toroidal Field Coil Short	IV	D

Table 2.2-6 VV Design Load Case Combinations and Categories

Operating State	ITER Load Category	Service Limit Level (per ASME Code)
1) Baking State + seismic (SL-1)	II	A
2) TFCFD + VDE I	I	A
3) TFCFD + CD I	I	A
4) Seismic (SL-1) + CD I	II	A
5) Seismic (SL-1) + VDE I	II	A
6) Seismic (SL-1) + TFCFD	III	C
7) Seismic (SL-1) + CD II	III	C
8) Seismic (SL-1) + VDE II	III	C
9) Seismic (SL-1) + TFCFD + CD II	III	C
10) Seismic (SL-1) + TFCFD + VDE II	III	C
11) Seismic (SL-2) + CD I	IV	D
12) Seismic (SL-2) + VDE I	IV	D

For normal operating conditions (category I and II events), the most severe loads are caused by the coolant pressure, VV and in-vessel component weights, seismic events, plasma

disruptions and VDEs, and the TF coil fast discharge (TFCFD). The loads that mainly drive the design are due to a centred disruption (CD), VDE, and a TFCFD. The maximum vertical and horizontal forces on the VV are reported in 2.12. Seismic loads on the VV are reported in 2.15. The main electromagnetic load conditions estimated for the VV are reported in Table 2.2-7. In the tables, M_r, M_p, F_r, and F_p represent the maximum radial and poloidal moments and forces on modules, respectively. Figure 2.2-14 shows the sign convention for forces and moments. Normal operation coolant pressure is 1.1 ± 0.2 MPa. Maximum internal and external VV pressure in off-normal events is 0.2 MPa. Component weights are defined in Table 2.2-1.

Table 2.2-7 Main Electromagnetic Load Conditions for VV

Event	Load Cat.	Max. EM Pressure on VV		Max. EM Loads on Blanket Module			
		P_r (MPa) due to Eddy Currents+++	P_r (MPa) due to Halo Currents	M_r (MNm)	M_p (MNm)	F_r (MN)	F_p (MN)
TFCFD	I	-1.6	-	-	-	-	-
CD II	II	0.1 ~ 1.2	-0.66	-0.71	0.57	-0.15	-0.39
VDE/S-D II	II	0.1 ~ 1.2	-2.9	-	-	0.20	0.67
VDE/S-U II	II	0.1 ~ 1.2	-1.1	-	-	-0.14	-0.28
VDE/F-D II	II	0.1 ~ 1.2	-1.7	-0.54	0.41	0.12	0.38
VDE/F-U II	II	0.1 ~ 1.2	-0.60	-0.55	-0.41	-0.08	-0.16
TFCFD + VDE/S-D I+	II	-1.6	-2.2	-	-	0.15	0.51
VDE/S-D III	III	0.1 ~ 1.2	-3.9	-	-	0.27	0.90
VDE/S-U III	III	0.1 ~ 1.2	-1.4	-	-	-0.18	-0.37
VDE/F-D III	III	0.1 ~ 1.2	-2.2	-0.72	0.54	0.15	0.50
VDE/F-U III	III	0.1 ~ 1.2	-0.81	-0.73	-0.54	-0.10	-0.21
TFCFD +VDE/S-D II++	III	-1.6	-2.8	-	-	0.19	0.64

\+ I_{halo}/I_{plasma} x TPF (toroidal peaking factor) = 0.348 (60% of the VDE III). B_{tor} is assumed to be $0.95B_{tor}(0)$ at the time of max. EM pressure due to TFCFD.

++ I_{halo}/I_{plasma} x TPF = 0.435 (75% of the VDE III). B_{tor} = $0.95B_{tor}(0)$.

+++ Pressure due to the eddy current induced by a CD has the opposite direction to the pressure due to halo current and TFCFD, and should be neglected in load case combinations.

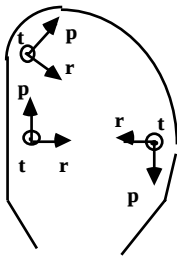

Figure 2.2-14
Local Coordinates

The upper and the equatorial ports are the most loaded constructions since the highest electromagnetic loads affect their in-port components during plasma events. The main loading conditions for these ports are summarized in Table 2.2-8. The data are given for the most loaded in-port components, namely for the EC-launcher for the upper port and the test blanket module for the equatorial port.

Table 2.2-8 Main Load Conditions for the Upper/Equatorial In-Port Components

Loading case/ port structure		Electromagnetic loads					Seismic loads			In-vessel pressure, MPa
		M_r, MNm	M_t, MNm	M_p, MNm	F_r, MN	F_p, MN	a_r, m/s^2	a_t, m/s^2	a_v, m/s^2	
EM I[1] + SL-1	Upper	1.2	1.3	0.26	-	-0.07	2.81	2.58	5.72	-
	Equat.	8.6	-	-0.4	0.6	-	2.4	2.24	1.72	
EM II[2] + ICE II	Upper	1.6	1.6	0.33	-	-0.09	-	-	-	0.2
	Equat.	10.0	-	-0.5	0.7	-	-	-	-	
EM II + SL-1	Upper	1.6	1.6	0.33	-	-0.09	2.81	2.58	5.72	-
	Equat.	10.0	-	-0.5	0.7	-	2.4	2.24	1.72	
EM II[3] + ICE III	Upper	2.1	2.2	0.43	-	-0.12	-	-	-	0.2
	Equat.	9.0	-	-0.7	0.6	-	-	-	-	
EM I + SL-2	Upper	1.2	1.3	0.26	-	-0.07	8.26	7.59	16.81	-
	Equat.	8.6	-	-0.4	0.6	-	7.07	6.6	5.06	

1. Maximum electromagnetic loads enveloping the Category I events
2. Maximum electromagnetic loads enveloping the Category II events
3. Maximum electromagnetic loads enveloping the Category III events

2.2.7.3 Structural Analyses of Main Vessel

2.2.7.3.1 Primary Stresses

The global FE model static analyses of the VV have been performed using two different models (see fig.2.2-15): model A and model B. Both models have been developed using the ANSYS code. Each model provides, other than the results of the global analysis, boundary conditions for carrying out different specific local detailed analyses (see Section 2.2.7.3.2).

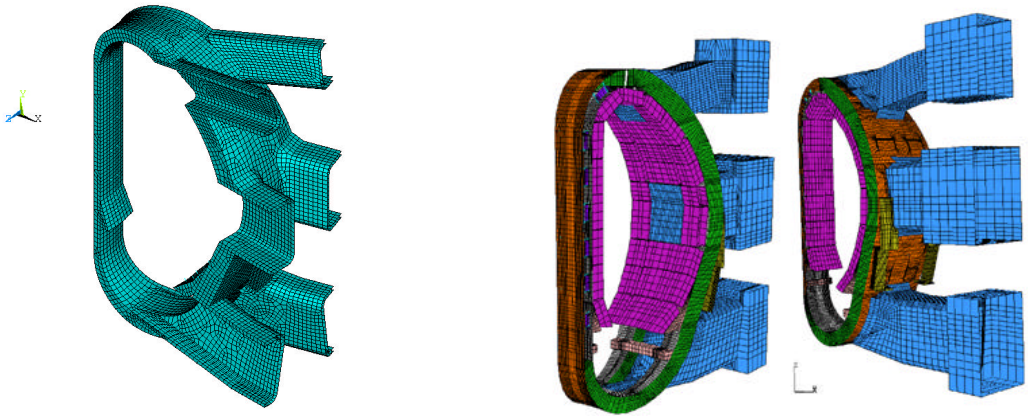

Model A **Model B**

Fig.2.2-15 Global FE Models Used for the Global Analyses of the VV

Table 2.2-9 reports a list of the analyses performed by the two models.

Table 2.2-9 List of the Global VV Analyses Performed by Two Different FE Models

	Model A	Model B
Global Vessel Analyses: Primary Loads		
Gravity (DW)	X	X
Operating Coolant Pressure (CP)		X
Baking Coolant Pressure (BCP)		X
Centre Disruption II (CD II)		X
Toroidal Field Coils Fast Discharge (TFCFD)	X	X
VDE III [1]	X	X
Seismic load (SL-1 and SL-2)	X	X
Internal VV Pressure 0.2 MPa		X
External VV Pressure 0.2 MPa		X
VDE II [1] + DW	X	
TFCFD + VDE I + DW + CP		X
VDE III [1] + DW	X	
SL-1 + VDE II +TFCFD	X	X [2]
SL-1 + CD II + TFCFD + CP		X

Notes:
1. VDE cases include slow, fast, upward and downward events.
2. Includes also coolant pressure

The definition of the worst case and load case combination depends on the VV region of interest.
The CD I and CD II events generate loads on the blanket modules that are generally smaller or similar to those caused by the fast VDE I and VDE II. In addition, CD events have halo current pressures that are smaller than those caused by the fast VDEs. For these reasons, the load case combinations TFCFD+VDE I and TFCFD+VDE II generally cause in the main VV, larger stress than the combinations TFCFD + CD I and TFCFD + CD II. A typical exception is the support structures of some blanket modules (i.e. the shear keys) that experience larger loads in the CD II events. For these regions the TFCFD+CD II event has to be considered as one of the worst load case.

The load case combinations SL-1+TFCFD, SL-1+VDE II, SL-1+TFCFD+VDE I, and SL-1+TFCFD+VDE II are all classified as category III (load service level C). The load case combination SL-1+TFCFD+VDE II is the one among these that generates the maximum stress in the VV.

As reported in Section 2.7.2.2, ICEs have to be combined with disruptions and VDEs. The VV internal pressure caused by the ICE occurs several seconds after the start of the leak. The disruption and VDE time scale is much shorter (less than a second), therefore, even if the ICE and plasma events are correlated, the associated loads never occur simultaneously and can be analyzed separately.

Among the events that are classified as category IV, the worst load case is represented by the combination SL-2+VDE I. This events generates larger stress than the combination SL-2+CD I, because, as stated previously, the halo current pressures in VDE I are larger than in CD I.

The load case combination SL-1+TFCFD+VDE II is characterized by larger EM loads than the combination SL2+VDE I and, in general, generates larger stress in the VV.

The SL-2 event generates large stress mainly in the VV support. The combination SL-1+TFCFD+VDE II, because it is classified as category III, has stress values that are closer to the allowable than the combination SL-2+VDE I, which is a category IV event.

In conclusion, the load case combinations that mainly drive the design of the VV are:

- TFCFD + VDE I
- SL-1 + TFCFD + VDE II

Seismic and EM loads have been combined applying equivalent static loads that take into account the dynamic effects (see Sections 2.2.7.3.3 and 2.2.7.3.4).

One of the most critical regions of the VV is the inboard wall because of the high toroidal field, which causes high EM forces. For this region the most severe loading conditions are the TFCFD and its load combination with EM loads due to a VDE, which cause high compressive stresses in the VV inboard wall and increase the risk of buckling.

An analysis of the VV structure performed to calculate the primary membrane and membrane plus bending stresses neglecting stress concentrations around discontinuities has given the results shown in Table 2.2-10. In the table P_m and P_m+P_b represent the membrane and the membrane + bending stress intensity. The most stressed region is the outer shell of the VV inboard wall.

Table 2.2-10 Primary Stress Intensity in the VV Inboard Wall

Event [1]	Load Cat	P_m (MPa)	Limit [2] (MPa)	P_m+P_b (MPa)	Limit [2] (MPa)
TFCFD	I	72	147	78	220
TFCFD+VDEI	I	129	147	180	220
SL-1 +TFCFD+VDEII	III	150	176	207	265

Notes:
1 Loads due to gravity and coolant pressure are included.
2 Limit for AISI 316 L(N) IG @ 150°C. In the welds a smaller limit value has to be assumed if the joint efficiency is lower than 1.

2.2.7.3.2 Detailed Local Stress Analysis

The VV structure has several geometrical discontinuities that cause localized stresses.

The structural analyses performed on the 3D global models have provided the boundary conditions for local detailed models. Several local detailed analyses have been performed to estimate the maximum local bending and peak stresses at these locations. The regions that have been analyzed in detail are:

- inboard wall : region around the support housings;
- lower and upper parts of the inboard wall region;
- inboard wall triangular support frame for the lower inboard blanket module;
- outboard wall region between the equatorial port and the lower port;
- VV support region.

Fig. 2.2-16 and -17 report some of the local detailed models used for the local analyses. The results of these local analyses show that the primary membrane and bending stresses are below the allowable values. The values of the estimated peak stresses do not indicate any risk of fatigue failure.

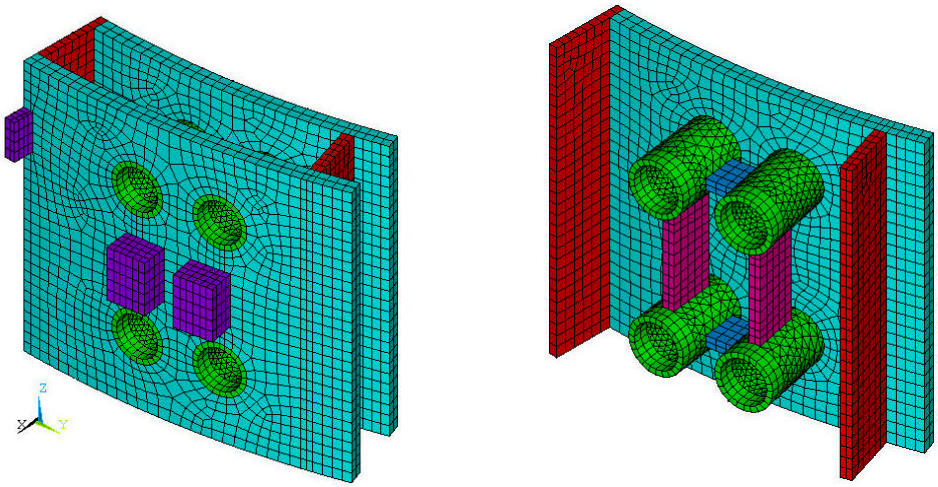

Fig. 2.2-16 Sub-Models Used for the Structural Analyses of the VV Inboard Wall

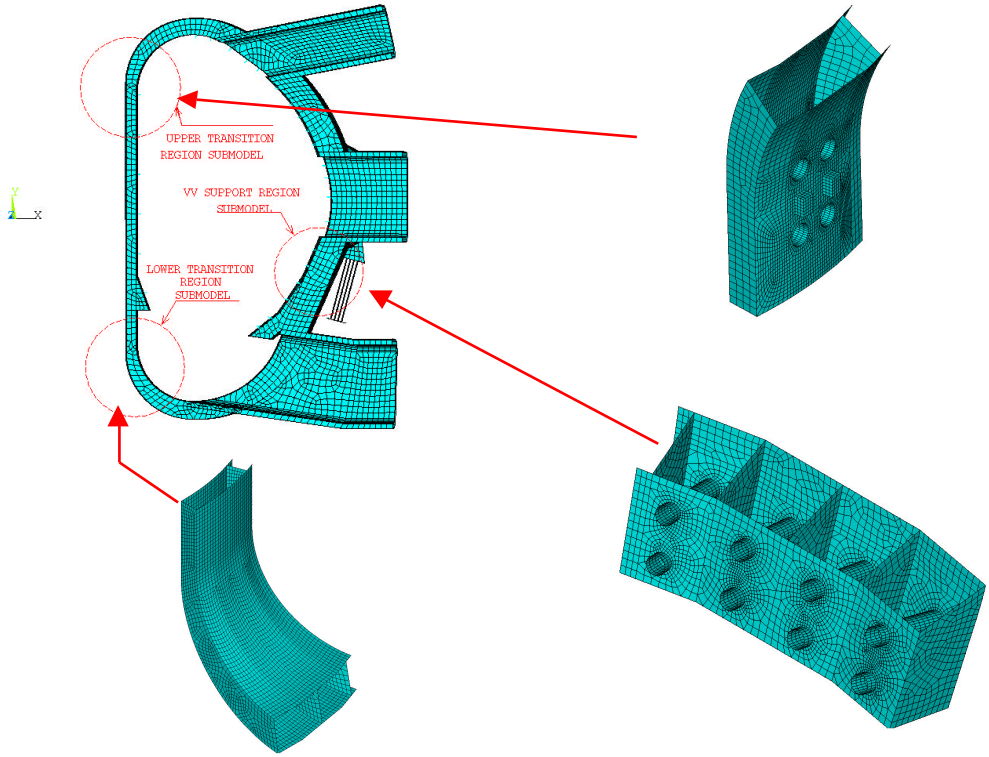

Fig. 2.2-17 Sub-Models used for the Structural Analyses of the Upper and Lower Cylindrical/Facet regions and the Outboard Region Below the Equatorial Port

2.2.7.3.3 Dynamic analysis

Due to the impulsive nature of the EM loads on the VV and in-vessel components in disruptions and VDEs, a dynamic analysis of the structure is required to understand the dynamic behavior of the VV and the dynamic amplification of the structure response for

different loading conditions. Different FE models have been developed for the dynamic analysis. The most important models and their main purposes are:

- Model A: a 20° sector model for the dynamic time-history analysis of the symmetric VDE and disruption cases;
- Model B: a 90° sector model for the modal analysis;
- Model C: a 180° sector model for the dynamic time history analysis of the asymmetric VDE cases.

All models have been developed using the ANSYS code. Figure 2.2-18 shows model A and C. Model B is derived from model A reflecting the model from 20° to 90°. Model A and B include the VV inner and outer shells, the poloidal and toroidal ribs, the ports, the cantilever plugs, the connecting ducts to the cryostat, the blanket modules and the VV supports. Divertor structure and other in-vessel components are modelled as "non-structural masses". Model C is a more simplified model with the main VV body (inner and outer shells, poloidal and toroidal ribs) modelled with an equivalent single layer shell.

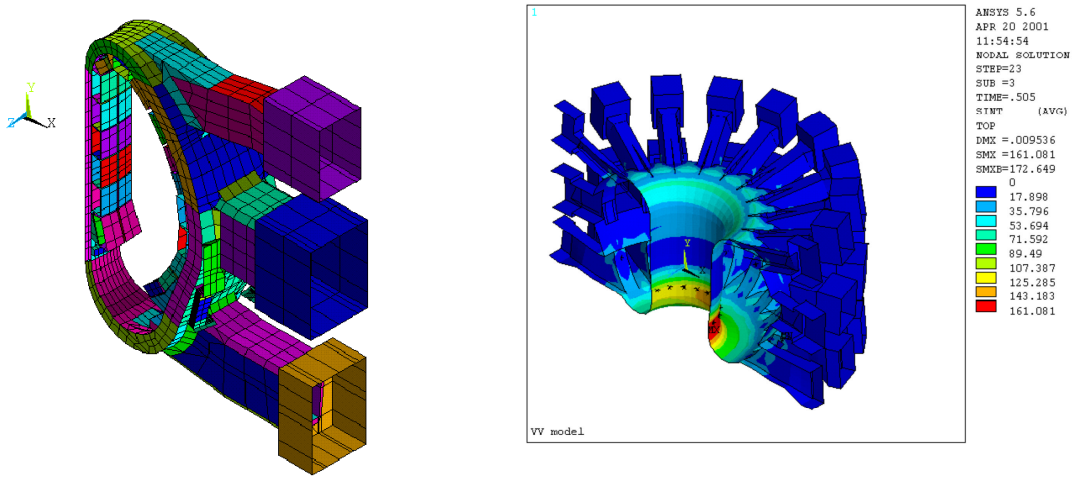

20° Sector Model **180° Sector Model with Stress Intensity (MPa)**

Fig.2.2-18 20° Sector Model and 180° Sector Model with Stress Intensity Contour Plot at Asymmetric VDE/S-D III Obtained at Time 505 s

Considering the results of the dynamic analyses performed on the 20° and the 180° models, the maximum expected vertical and horizontal forces in a VDE/S-D III on a single VV support are 6.0 MN and 4 MN respectively, which indicate that the vertical and horizontal forces on the supports in VDEs are dynamically amplified by factors equal to 1.2 and 1.4 respectively.

The largest displacement of the VV main body and ports have been obtained from the 180° model which includes the effects of the net horizontal force on the VV. Maximum values occur in a VDE/S-D III. The maximum displacements of the upper port plug occur in the VDE/F-U III. The VDE/F-U III has also given the maximum relative displacements of the port plugs with respect to the VV.

Table 2.2-11 reports a summary of the maximum displacements at different locations.

Table 2.2-11 Summary of the Results of the Dynamic Analysis: Maximum Absolute and Relative Displacements in VDE III [1]

Location	Displacements (mm)		
	Radial	Vertical	Toroidal
Top of VV	3.0	6.1	2.1
Inboard Wall	3.6	8.0	2.7
Bottom of VV	3.0	7.2	2.1
Outboard wall	2.4	0.62	1.6
End of Port Duct of Upper Port	4.7	5.0	2.2
End of Port Duct of Equat. Port	2.5	2.4	1.4
End of Port Duct of Lower port	3.5	4.1	1.1
Upper Port Plug (or Antenna)	2.6	4.8	7.9
Equat. Port Plug (or Antenna)	1.8	0.35	1.4
Relative Displacement Upper Port Plug/VV	1.9	2.7	7.6
Relative Displacement Equatorial Port Plug/VV	0.6	0.7	0.64

[1]. Maximum values do not occur at the same toroidal location and for the same type of VDE

The maximum membrane stress in the VV shell occurs at the inboard wall in the VDE/S-D III. The results of the dynamic analysis show that the amplification factor for this value is equal to 1, which means that the detailed stress analysis of this region (see Section 2.2.7.3.1) can be performed by a static analysis applying the EM loads without any dynamic amplification.

2.2.7.3.4 Seismic analysis

Two independent seismic analyses have been performed with different aims:

- analysis A is orientated at getting results for the whole tokamak machine;
- analysis B is oriented at getting more accurate results for the VV.

The FE model used in the analysis A represents the VV using a single layer shell having a stiffness equivalent to the double shell wall with ribs. The analysis A is described in Section 2.15. The FE model used in the analysis B has a more accurate representation of the inner and outer shells and the poloidal and toroidal ribs.

The FE models used for the seismic analyses have been developed at different stages of the ITER design and for that reason each analysis is somewhat different. Results comparisons and parametric studies showed that it is very important to represent correctly the local stiffness especially at the connections between components. For some tokamak components, most of the flexibility is concentrated at these locations. An incorrect modelling of these connections can cause inaccuracy of the results.

The natural frequencies have been determined as a part of both analyses. The modes making the largest contribution in the horizontal and vertical directions are summarized in Table 2.2-12. The results are in relatively good agreement.

Table 2.2-12 Tokamak Natural Frequencies (1,2)

	Natural frequency (Hz)			
	Analysis A		Analysis B	
	Horiz.	Vertical	Horiz.	Vertical
First natural frequency of the tokamak	2.8	8.3	2.4	8.8
First natural frequency of the VV and in-vessel components	6.4	9.7	4.8 (3)	11.1

1. The VV natural frequencies have been obtained excluding the magnets from the model (VV vertical and horizontal supports at the attachments to the TF coils are restrained in all directions).
2. Vertical modes are obtained applying symmetry constraints to the nodes of the VV on the vertical boundary planes. Horizontal (toroidal) modes are obtained applying anti-symmetry constraints to the nodes of the VV on the vertical boundary planes.
3. A value of 5.5 Hz has been obtained assuming a more rigid connection between the VV support flanges.

The two seismic analyses give the maximum vertical and toroidal forces on the VV supports in the SL-2 case as shown in Table 2.2-13. These values are used for the structural analysis of the VV supports performed using more detailed models and including loads from other sources (see load combinations list in table 2.2-6).

Table 2.2-13 Maximum Reaction Forces on a Single VV Support for a SL-2 Load

Analysis A		Analysis B	
Toroidal Force (MN)	Axial Force [1] (MN)	Toroidal Force (MN)	Axial Force [1] (MN)
9.2	4.6	8.5	3.5

1. The axial direction corresponds to the axis of the VV support plate, which is inclined with respect to the vertical axis of the machine by 15°

The results for an SL-1 earthquake can be obtained from the SL-2 results scaling the values by a factor 0.34. This factor comes from the consideration that SL-2 has a ground peak acceleration of 0.2g, while the SL-1 value is 1/4 of it (0.05g). In addition SL-2 has a larger damping.

Seismic loads generate relatively small stress in the main VV body, apart from the support regions. The stress analysis of the VV (see section 2.2.7.3.1) for the seismic load is performed applying an equivalent static load (a static load that generates the same stress as expected in the seismic event). This method allows:

- a more detailed FE model for the stress analysis
- the combination of the seismic loads with other applied loads (as listed in table 2.2-6 and 2.2-9).

2.2.7.3.5 Buckling Analyses

In the case of a TFCFD, the induced poloidal currents in the VV interact with the toroidal magnetic field causing compressive stress in the VV inboard wall. Elastic buckling analysis has shown that the critical elastic buckling pressure is much larger than the pressure that causes a stress level above the yield. An assessment of the inelastic buckling has given a minimum load for buckling of 6.6 MPa for the VV in the case of the TFCFD load distribution. The VV geometrical imperfections that have minimum critical inelastic pressure are the radial misalignment of adjacent sectors (the mismatch ±5 mm is compensated by the splice plate) and the imperfection congruent with the first elastic buckling mode (mode m = 6). A sensitivity study on the effect of the increase of the initial

imperfection of the VV geometry from ± 5 mm to ± 10 mm has given a reduction of the critical pressure of ~ 4%. It is assumed that the load factor (ratio between the buckling load and the applied load) is higher than 2.5 for categories I and II[1]. The maximum EM pressure during a TFCFD is 1.6 MPa, which gives a load factor of 4.1.

The inelastic buckling analyses performed for the load case combinations TFCFD + VDE I has given a load factor (LF) equal to 2.5, which is the minimum allowable.

As a consequence, to prevent the structural buckling of the VV inboard wall and to keep the primary stresses below the allowable values, the support frame for the modules in the inboard-bottom region needs to be a toroidally continuous structure.

An assessment of the effect of the support housings and the geometrical discontinuities caused by the module direct attachment to the VV has shown that the support housings do not reduce the buckling inelastic strength of the VV inboard wall. This conclusion has been obtained comparing the results from two FE models: one which includes the support housings and one without the support housings.

2.2.7.3.6 Thermal Stress due to Nuclear Heat Load

The thermal stress in normal operation is generated mainly by the nuclear heating. The nuclear heat load on the surface of the inner shell of the VV on the plasma side is equal to 0.1 W/cm^3 in locations behind the blanket modules (module thickness = 450 mm). The installation and handling procedure of the blanket modules requires the presence of gaps between modules. In the current design, these gaps are filled by the manifolds of the blanket coolant which provide a partial shielding and reduce the nuclear peak load to an estimated value of 0.4 W/cm^3 (see Table 2.2-14). A study on the effect of the heat transfer coefficient (HTC) between the VV coolant and the VV shell in steady state has shown that the thermal stress increases considerably if this coefficient is lower than 500 W/m^{2}K (see Figure 2.2-19). Assuming this value for the HTC, the highest temperature of the vessel structure is about 161˚C (water coolant temperature = 100˚C; nuclear heating rate = 0.4 W/cm^3) and the thermal stress is 175 MPa. Assuming that the maximum primary stress for category I and II events is 180 MPa (see Table 2.2-10), the maximum stress range obtained by the combination of the thermal and the primary stress is not expected to exceed the allowable ($3S_m$ = 441 MPa). The thermo-hydraulic analysis (see 2.2.7.6) has shown that the HTC is > 500 W/m^{2}K even in natural convection (no forced flow) in the inboard and outboard wall (see Figure 2.2-20 – "0-degree" curve) where the nuclear heating is maximum (see Table 2.2-14).

High thermal stress can be generated even in relatively small structures attached to the VV inner shell (i.e. shear and stub keys, divertor support rails) if not actively cooled or properly shielded.

[1] RCC-MR, "Design and Construction Rules for Mechanical Components of FBR Nuclear Islands."

Table 2.2-14 Nuclear Heating Rate on VV Interior Surface

Location	Average (MW/m^3)	Peak (MW/m^3)
Inboard wall	0.1	0.3
Top of the VV	0.083	0.25
Outboard wall	0.15	0.4
Bottom of the VV	0.045	-

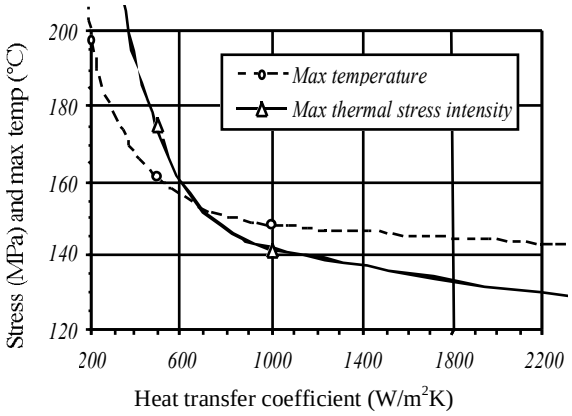

Figure 2.2-19 Effect of Cooling Capability on VV Thermal Stress

2.2.7.4 Structural Analyses of Port Structures

Several static structural analyses have been performed to calculate the stresses/strains for the port structures. The stresses and displacements for the upper and the equatorial ports are summarized in Table 2.2-15 for the worst loading conditions taken from the Table 2.2-8.

Table 2.2-15 Maximum Stresses and Displacements for Equatorial Port Structure

Location		Primary Membrane Stress (MPa)		Primary Membrane plus Bending Stress (MPa)		Maximum Displacement (mm)	
		Upper Port	Equatorial Port	Upper Port	Equatorial Port	Upper Port	Equatorial Port
In-port component	Inner shell	70	70	95	92	0.7	0.8
	Outer shell	100	70	155	97	0.8	0.9
	Ribs	60	70	85	91	0.7	0.8
Port extension	Inner shell	80	85	115	122	0.7	0.5
	Outer shell	35	40	50	62	0.8	0.5
	Ribs	70	45	86	63	0.7	0.5

The maximum primary membrane stresses are 85 MPa and 100 MPa for the port extension and the in-port component, respectively (the stress limit is 147 MPa), and the maximum membrane plus bending stresses are 122 MPa and 155 MPa (the stress limit is 221 MPa). These stresses occur in the areas near to tangential keys, and the stresses in all other areas are much lower. The maximum average contact stress in the key is about 65 MPa for the upper port (maximum stress intensity is 140 MPa), and 230 MPa for the equatorial port (maximum stress intensity is 362 MPa). The maximum stresses are generally below the stress limits. To increase the safety margins, the keys may be manufactured from a stronger material than SS 316 L(N) (e.g., a stainless steel A-286 (AISI 660) that is about twice as strong as SS 316 L(N)).

The static analyses of the ports performed on detailed models, which include the ports and in-port components (attachment points to the VV are assumed fixed) have given maximum displacements of the in-port component ends in the front portion equal to 5.3 mm for the upper port and about 1.4 mm for the equatorial port. These rather small displacements

confirm the feasibility of the cantilever concept. At the back of the port structure, the maximum relative displacement between the port and the in-port component is about 0.1 mm for the upper port and about 0.4 mm for the equatorial port. The latter displacement causes a deformation of the lip-welded joint but resulting stresses are well below the stress limit.

A structural response to the dynamic character of the electromagnetic load application has been also assessed. For this assessment, the maximum accelerations calculated as a result of the VV dynamic analysis (namely, a radial acceleration of 0.3g, a vertical acceleration of 0.6g, and a toroidal acceleration of 4.5g) were applied to the upper port model. The maximum primary membrane stresses are 105 MPa and 110 MPa for the port extension and the in-port component, respectively, and the maximum membrane plus bending stresses are 148 MPa and 163 MPa. The maximum average contact stress in the key is about 45 MPa (the maximum stress intensity is 175 MPa). These values are below the allowables.

2.2.7.5 Operation at 17 MA Plasma Current

The increase of the electromagnetic loads due to an increase of plasma current from 15 MA to 17 MA reduces the stress safety factor for primary loads to values very close to 1. If a joint weld efficiency of 1 is not achieved for some joints (e.g. the one-sided field joint) the primary stress might exceed the allowable values at few locations.

Preliminary buckling analysis has shown that for the present VV design the buckling safety factor is 2.3 for the load case combination TFCFD + VDE I in case of 17 MA operation, which is slightly smaller than the allowable value (following the RCC-MR code[1] the allowable value is 2.5). Therefore, before operating at 17 MA, plasma conditions have to be experimentally ascertained to modify the currently considered conservative assumptions (so that less conservative assumptions can be used for the VV structural analyses).

2.2.7.6 Thermal and Hydraulic Analysis

A series of thermal and hydraulic analyses of the VV have been conducted to clarify the heat balance without any peaked heat in the VV and heat removal capability both during normal (forced convection cooling mode) and off-normal (natural convection cooling mode) operations. As discussed in 2.2.7.3.4, it is expected that the maximum nuclear heating caused by direct neutron streaming between the modules will be approximately four times higher than the average heating rate (~ 0.1 W/cm^3) of the VV inner shell. In order to keep the thermal stress of the VV below the allowable, a sufficient heat removal capability, such as ~ 500 W/m^2K of heat transfer coefficient on the wall surfaces, is required for the VV cooling (see 2.2.7.3.4). Such a heat removal capability can be achieved if forced flow cooling with a flow velocity > 0.05 m/s is used. However, the overall water mass flow rate needs to be minimized to keep the required heat transfer system as small as possible.

Since the flow velocity of the water is not so high even for normal operation, it is expected that natural thermo-gravitational convection due to the heat flux from the vessel wall to the water will enhance the heat transfer characteristics (i.e., the forced convection heat transfer). Figure 2.2-20[2] shows an example of the calculated heat transfer coefficient as a function of

[1] RCC-MR, "Design and Construction Rules for Mechanical Components of FBR Nuclear Islands."
[2] M. Onozuka, et al., "Design and Thermal/Hydraulic Characteristics of the ITER-FEAT Vacuum Vessel," in Proc. 21st Symposium on Fusion Technology, Madrid, Spain, September 11-15, 2000.

the flow velocity, where "degrees" indicates inclination angle to the vertical for mixed convection flow. It was assumed that the water temperature is 100˚C and the heat generation is 0.1 W/cm^3. An enhanced heat transfer capability due to natural convection is expected for a flow velocity lower than 0.06 m/s. To confirm the effect of the natural convection on the thermal and hydraulic characteristics of the VV and to reduce the overall water mass flow rate, experimental investigation will be required.

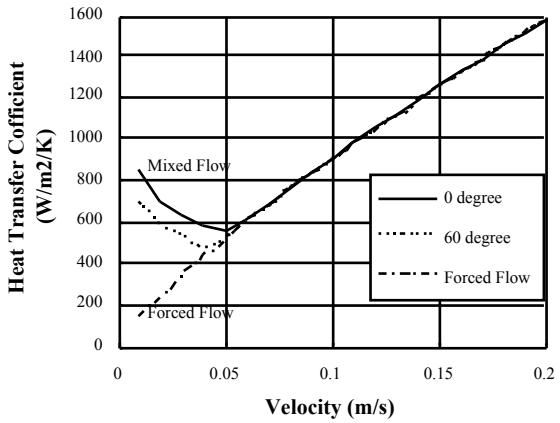

Figure 2.2-20 Heat Transfer Characteristics for VV Coolant Channel

2.3.8 Vacuum Vessel Overall Assessment

The VV must withstand many individual and combined loading conditions during both normal and off-normal operation. Analyses done to date are those considered to be the most severe loading cases, which will drive the basic design of the VV structure. Although further analyses are required for numerous loading conditions to confirm the structural integrity of the VV, based on the analyses performed to date, the VV appears structurally capable of withstanding the expected loads.

The main emphasis of the continued design development up to the procurement will be to refine the procurement specification used for the cost estimation in the detail necessary for procurement tendering to be launched at the start of the construction phase. This will include the development of any necessary technical justification to allow the design to be licensed in any of the potential ITER host countries including the code qualification of vessel features which are not fully covered by or comply with existing codes.